



# Synthesis of polyaniline/graphene composite and its application in zinc-rechargeable batteries

Zhen Wang<sup>1</sup> · Jia-Jun Han<sup>1</sup> · Ning Zhang<sup>1</sup> · Dan-Dan Sun<sup>1</sup> · Tao Han<sup>1</sup>

Received: 15 July 2019 / Revised: 25 October 2019 / Accepted: 25 October 2019 / Published online: 18 November 2019  
© Springer-Verlag GmbH Germany, part of Springer Nature 2019

## Abstract

Polyaniline, polyaniline/graphene composites were synthesized by a novel in situ chemical oxidative polymerization method including two oxidants. The morphology and structure of the material were characterized by field emission scanning electron microscopy (FE-SEM), transmission electron microscopy (TEM), X-ray diffraction (XRD), and Fourier transform infrared spectroscopy (FT-IR). The electrochemical performance of polyaniline (PANI)-based composites was tested by electrochemical impedance spectroscopy (EIS), cyclic voltammetry (CV) testing, and constant current charge and discharge (GCD) tests. At 0.2 C of constant current, the discharge specific capacities of PANI/graphene oxide (PANI/GO) and PANI/GO-sodium borohydride (graphene oxide is reduced by sodium borohydride, named PANI/GO-NaBH<sub>4</sub>) were as high as 183 mAh/g and 192 mAh/g, respectively, which was nearly twice as high as that of PANI (100 mAh/g). After 100 charge and discharge cycles, the capacity retention rates of PANI, PANI/GO, and PANI/GO-NaBH<sub>4</sub> were 80.4%, 89.4%, and 95.05%, respectively; the cycle performance was greatly improved before the modification. These results indicate that the composite has exciting potentials for the cathode material of zinc-rechargeable battery.

**Keywords** Polyaniline · Zinc · Graphene · Chemical oxidation polymerization · High specific capacity

## Introduction

In recent years, the rapid development of industry has caused serious consumption of non-renewable resources such as coal, oil, and natural gas. The global warming and the energy crisis caused by the use of fossil fuels are the biggest challenges in this century; it is important to develop high-efficiency energy storage devices with extremely high safety and low cost [1–3] for resolving these challenges. Lithium-ion batteries (LIBs) have attracted considerable attention due to their recharging ability and high energy density [4, 5]. However, lithium-ion batteries are expensive and explosive [6], and organic electrolytes can pollute the environment. In addition, lead-acid batteries not only have low energy density and limited service life but also cause serious environmental problems [7, 8].

Metal zinc has a low redox potential (0.76 V relative to a standard hydrogen electrode), a high theoretical capacity

(5845 mAh/cm<sup>3</sup>, 819 mAh/g), and has good compatibility with water, making it a convenient anode for aqueous batteries [9, 10]; it has abundant reserves, non-toxicity, and air stability on the earth further facilitate large-scale production. At present, zinc rechargeable batteries have been well developed, such as zinc/manganese batteries [11, 12], zinc/polymer batteries [13, 14], and zinc/air batteries [15–17].

Zn/polyaniline (PANI) batteries are ecologically acceptable, low cost, and simple fabrication compared with conventional batteries [18–20]; they are a typical Faraday electrode material. The Zn/PANI rechargeable battery uses an aqueous electrolyte and has an overall environmental friendliness, low cost, and high theoretical specific capacity. The PANI materials synthesized by the common method are relatively agglomerated, which makes the utilization rate of PANI reduced [19, 21]; only the outer layer material can be in contact with the electrolyte. The PANI electrode undergoes volume expansion and contraction, which results in mechanical degradation of the electrode, resulting in reduced capacity and reduced cycle performance.

Graphene [22–24] is a two-dimensional (2D) crystal structure with sp<sup>2</sup> hybrid carbon atom arrangement. Due to its unique properties, graphene has high electron mobility at

✉ Jia-Jun Han  
hanjiajunhitweihai@163.com

<sup>1</sup> School of Marine Science and Technology, Harbin Institute of Technology, Weihai 264209, China

room temperature, excellent thermal conductivity and extraordinary mechanical properties, higher specific surface area, and the like, but the surface of graphene has no chemical functional groups, which impairs its dispersibility in the matrix and limits its application. Graphene oxide (GO) not only has the excellent properties of graphene but also many oxygen-containing groups (such as  $-\text{COOH}$ ,  $-\text{C}=\text{O}$ , and  $\text{OH}$ ) on the surface of graphene oxide make graphene oxide a highly porous adsorbent [25, 26]. In addition, GO has good solubility in solvents [27], which provides a lot of opportunities for building GO-based hybrid nanocomposites. PANI and GO can be intertwined by  $\pi$ - $\pi$  stacking, hydrogen bonding, electrostatic interaction, and can effectively reduce the agglomeration of PANI. At present, the composite materials of graphene and PANI are widely used in supercapacitors [28–30] and lithium PANI-rechargeable batteries [31], but there are few studies in Zn/PANI-rechargeable batteries.

Zn/PANI batteries have higher theoretical specific capacity, but the actual capacity is only a few tens of mA. This is due to the serious agglomeration of PANI during the synthesis process. In this paper, PANI and PANI/graphene composites are synthesized by adsorption double oxidant method. PANI is modified by using graphene oxide to make PANI polymerized with the graphene (graphene is as a template) to synthesize 3D mixed nanostructures, which weakens the agglomeration of PANI to accelerate the dedoping of ions during electrochemical reaction, and increases the specific capacity [32].

## Experimental

### Chemicals and materials

Aniline (AN), ammonium persulfate (APS), triton, ammonia, hydrochloric acid (37% HCl), sulfuric acid ( $\text{H}_2\text{SO}_4$ ), sodium nitrate ( $\text{NaNO}_3$ ), potassium permanganate ( $\text{KMnO}_4$ ), manganese dioxide ( $\text{MnO}_2$ ), sodium borohydride ( $\text{NaBH}_4$ ), natural graphite powder, activated carbon, and anhydrous alcohol are all analytical grade chemicals and purchased from the National Pharmaceutical Group Chemical Reagent Company, No. 52 Ningbo Road, Shanghai, China. Acetylene black is battery grade, purchased from Aladdin, Y891 (Branch), Fengxian District, Shanghai, China.

### Preparation of PANI-based composites

#### Preparation and reduction of graphene oxide

Graphene oxide (GO) was synthesized by using the modified Hummers method [33, 34]. The dispersion containing 0.5 g of GO was diluted to 500 mL; 5 g of  $\text{NaBH}_4$  was slowly added; the solution was stirred at 80 °C for 1 h in a water bath,

followed by centrifugation. Finally, low oxidation degree graphene oxide ( $\text{GO-NaBH}_4$ ) was obtained.

### Synthesis of PANI and PANI /Graphene composites

**Synthesis of PANI** In this paper, PANI is synthesized by adsorption double oxidant chemical oxidation method, and this method is economical, so it is suitable for mass production.

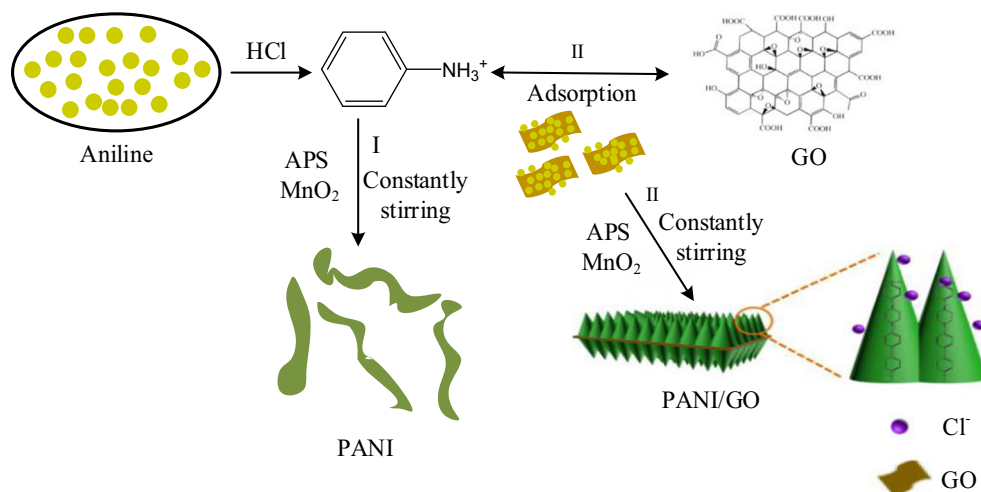
An amount of 4.68 g of  $\text{MnO}_2$  was added to the beaker, and 28.57 g of 0.1 mol/L  $\text{H}_2\text{SO}_4$  solution was added, stirred for 0.5 h, and the seal was transferred to the upper layer of the refrigerator. Two hundred fifty grams of deionized water, 85.72 g of concentrated HCl, and 0.25 g of triton were sequentially added to a 10000-mL reactor. The seal was stirred for 0.5 h. An external cooling system was set up, and 50 g of aniline was added to the reaction vessel and stirred for 1 h. Seventy-two grams of deionized ice was added to keep the temperature in the reactor below 5 °C, then 7.86 g of APS was added, and the activated  $\text{MnO}_2$  was stirred for 1 to 2 min and then added to the reaction vessel. A total of 1.07 g of APS was added in 1 min for a total of 120 times; during this process, we need to control the temperature below 5 °C. After the addition of APS, the reaction was carried out for 3 h, suction filtered, and washed 4 times with deionized water. Fifty grams of wet powder was added to ammonia water, sealed, stirred at 45 °C for 24 h, suction filtered, and washed with deionized water until neutral to obtain eigenstate PANI. Fifty grams of eigenstate wet powder was added to 0.2 mol/L perchloric acid solution, and the mixture was stirred at a constant temperature in a 45 °C water bath for 24 h, filtered, washed until the pH of the filtrate was greater than 5, and dried in a blast drying oven at 60 °C for use.

**Preparation of PANI/graphene composites** The preparation process of PANI/graphene composite material is shown in Fig. 1. The preparation process of PANI/GO composite (PANI/GO- $\text{NaBH}_4$  composite) is similar, except that GO ( $\text{GO-NaBH}_4$ ) is added during the process of synthesizing PANI while adding 250 g of deionized water, followed by 1 h of sonication. The next step is exactly the same. GO ( $\text{GO-NaBH}_4$ ) was added in order to polymerize aniline using graphene as a template to weaken the aggregation of PANI.

### Structure and morphology characterization

The X-ray diffraction (XRD) spectra were recorded on a D/X2700 diffractometer (Dandong Haoyuan Instrument Co., Ltd., China) with  $\text{Cu K}\alpha$  radiation. The morphology and observation were performed on field emission scanning electron microscopy (FE-SEM MERLIN Compact, Zeiss, Germany)

**Fig. 1** Preparation process of PANI and PANI matrix composites



and transmission electron microscope (TEM JEOL-2100, Electronics Co., Ltd., Japan). FTIR spectra were obtained by using a Nicolet 380 FT infrared spectrometer (US Thermo Electron Corporation, USA) from 2000 to 500  $\text{cm}^{-1}$ . XPS measurements were performed on an ESCALAB 250Xi spectrometer (Thermo Fisher Scientific, UK).

### Electrode fabrication and electrochemical measurements

First, we milled the prepared PANI for 15 min. Then, the PANI dry powder was fixed on a stainless steel mesh (diameter 14 mm) by roll pressing using the viscosity of PANI, so the electrode was completed, and we need to control the mass of the active material on the electrode to be about 15  $\text{mg}/\text{cm}^2$ . Finally, the prepared electrode is placed in a vacuum-drying oven and dried at 60  $^{\circ}\text{C}$  for 12 h.

The electrochemical measurements were performed in a two-electrode cell. To evaluate the electrochemical performances of these electrode materials, the working electrodes was a piece of material made by rolling onto a stainless steel mesh; the zinc sheet acted as a counter electrode. The membrane is made of glass fiber paper with a thickness of 0.8 mm and a diameter of 19 mm, and the electrolyte is 1.5 mol/L  $\text{ZnClO}_4$  and 0.5 mol/L  $\text{NH}_4\text{ClO}_4$  solution. Cyclic voltammetry (CV), electrochemical impedance spectroscopy (EIS), and galvanostatic charge–discharge (GCD) were performed via CHI660E electrochemical workstation (CHI660E, Shanghai Chenhua Device Company, China). The CV was carried out between 0.3 V and 1.7 V at a scan rate of 0.5  $\text{mV}/\text{s}$ . The battery was charged and discharged at 100  $\text{mA}/\text{g}$  for 10 cycles and then allowed to stand for 4 h before the electrochemical impedance test; the amplitude was 5 mV, and the frequency range was  $10^4\text{--}10^{-2}$  Hz. Galvanostatic discharge curves were performed on a LAND-CT2001A cycle life tester (Wuhan Jinnuo Instrument Co Ltd., Wuhan, China) between 0.7 V and 1.55 V. All measurements were carried out at room temperature.

## Results and discussion

### Structures and morphologies

Figure 2 shows the FT-IR spectrum of PANI, PANI/GO, and PANI/GO- $\text{NaBH}_4$  composites. The spectrum analysis shows that the characteristic absorption peaks of PANI are mostly between 500  $\text{cm}^{-1}$  and 2000  $\text{cm}^{-1}$ . Because the material is doped with perchloric acid, the peak shape is wider, and the peak intensity is weaker, but there are also obvious characteristic absorption peaks at 772  $\text{cm}^{-1}$ , 1020  $\text{cm}^{-1}$ , 1232  $\text{cm}^{-1}$ , 455  $\text{cm}^{-1}$ , and 1557  $\text{cm}^{-1}$ . Among them, the absorption peaks of 1557  $\text{cm}^{-1}$  and 1455  $\text{cm}^{-1}$  correspond to the C=C double bond stretching vibrations on the anthracene ring and the benzene ring, and the stretching vibrations corresponding to CN and C=N at 1232  $\text{cm}^{-1}$  and 1020  $\text{cm}^{-1}$ , respectively. These two functional groups are characteristic absorption peaks of PANI. The peak at 772  $\text{cm}^{-1}$  corresponds to the stretching vibration of C-C [35, 36]. Similar to PANI, the PANI-based

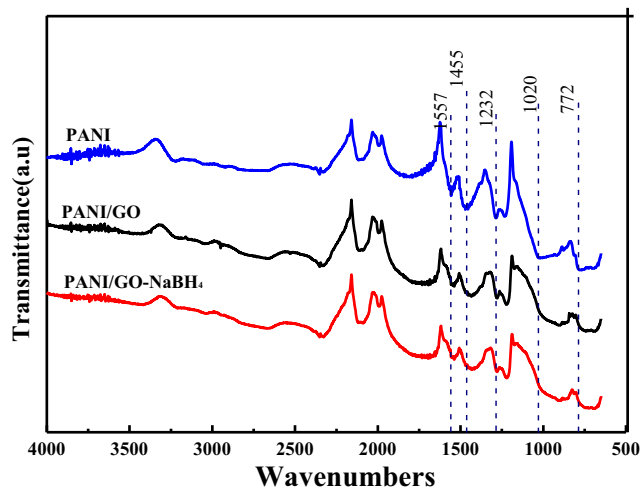


**Fig. 2** FT-IR spectrum of PANI and PANI/graphene composites (PANI, PANI/GO, and PANI/GO- $\text{NaBH}_4$ )

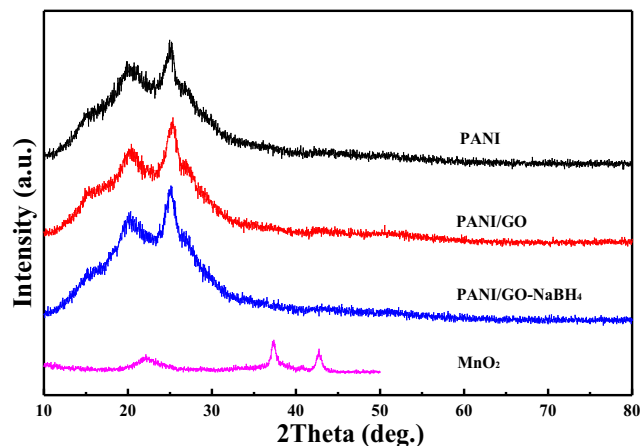


**Fig. 3** XRD pattern of PANI and PANI/graphene composites (PANI, PANI/GO, PANI/GO-NaBH<sub>4</sub>, and MnO<sub>2</sub>)

composites also showed very similar peaks in the peak shape, which indicates that the material structure of PANI did not change significantly after the composite with graphene, but the peak position has a little bit offset. The C=C stretching vibration of the corresponding PANI at 1557 cm<sup>-1</sup> and 1455 cm<sup>-1</sup> corresponds to the C=C stretching vibration in the PANI/GO composite to 1538 cm<sup>-1</sup> and 1434 cm<sup>-1</sup>. The  $\pi$ - $\pi$  interaction and hydrogen bonding between the skeleton of GO and PANI lead to the redshift of the spectrum, resulting in the delocalization of the charge along the PANI chain. The characteristic peaks of PANI/GO-NaBH<sub>4</sub> and PANI are also basically the same.

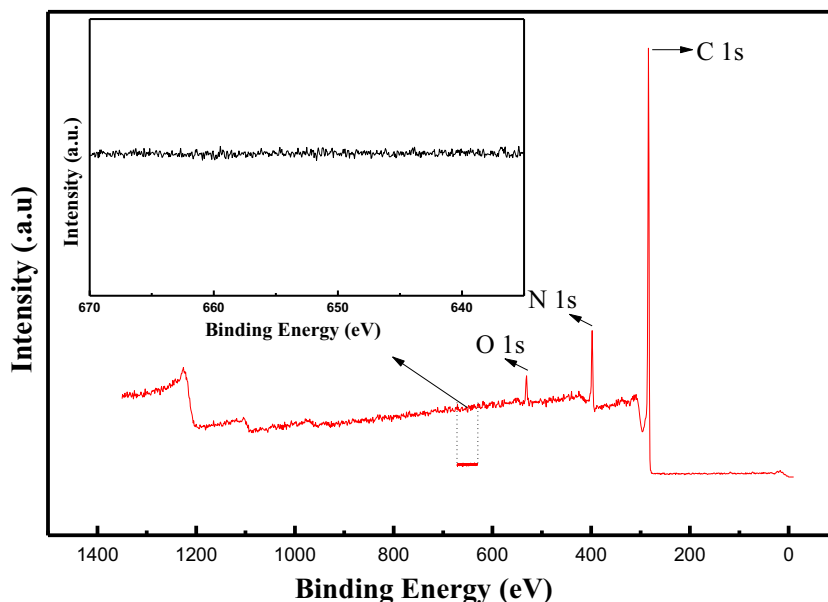
The crystal structure of PANI and PANI/graphene composites was detected by the XRD test. The XRD patterns of PANI, PANI/GO, PANI/GO-NaBH<sub>4</sub>, and MnO<sub>2</sub> are shown in Fig. 3. It can be seen that the XRD curve of PANI indicates that PANI has a partial crystal structure; two broad peaks are observed at

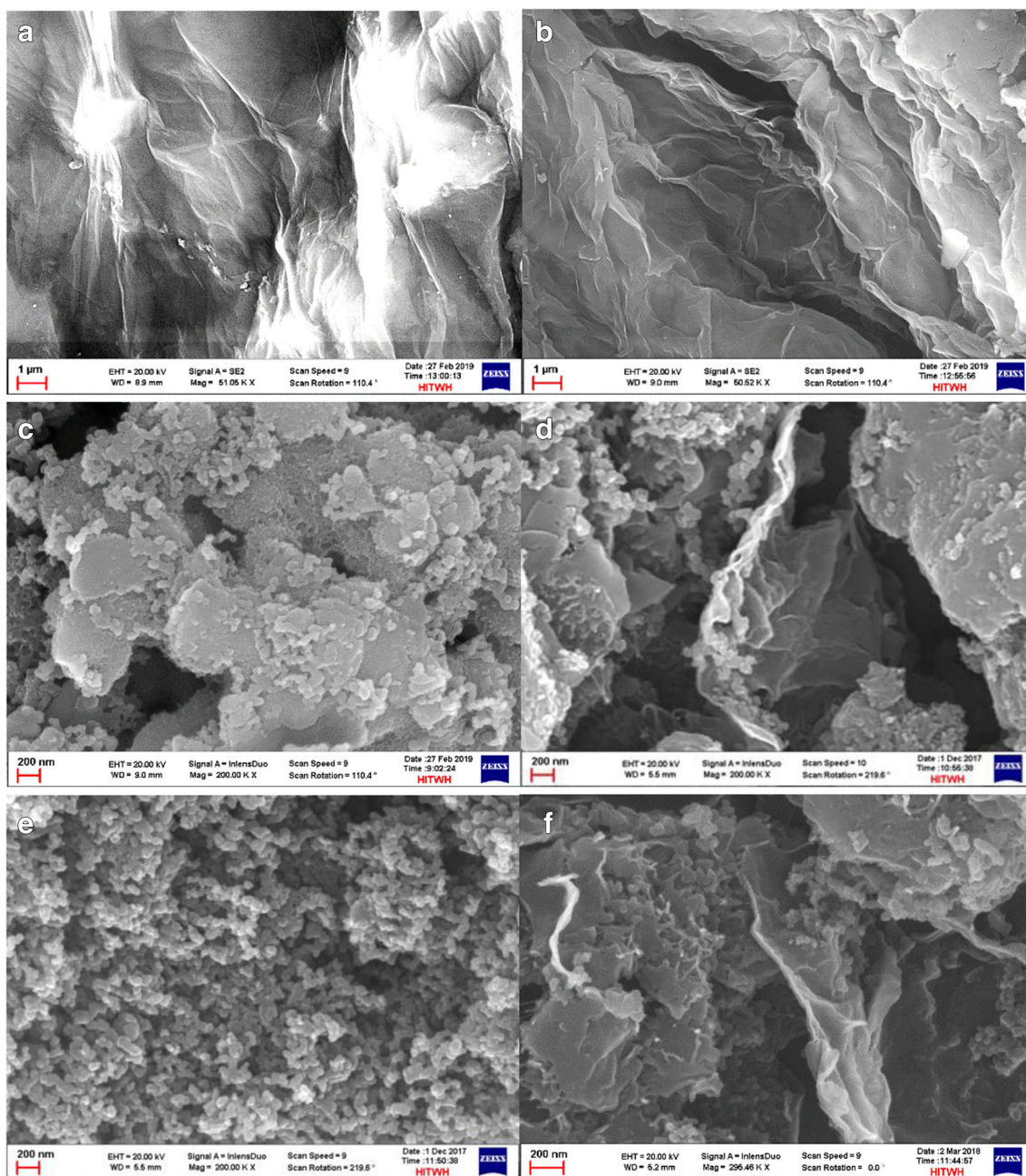
$2\theta = 19.8$  and  $25.61^\circ$ , and a less obvious Bragg diffraction peak at  $15.2^\circ$  corresponds to the emeraldine crystal faces of (020), (200), and (011), respectively [37]. After incorporation of 2% GO and GO-NaBH<sub>4</sub>, aniline was polymerized with graphene as a template. Due to the small doping amount, the XRD pattern peak shape of the material did not change significantly, but the diffraction peak corresponding to  $25.61^\circ$  became sharper. This proves that well-dispersed GO and GO-NaBH<sub>4</sub> favor the regular arrangement of PANI and improve the crystallinity by providing surface sites for PANI deposition, indicating that PANI and graphene are well combined together through  $\pi$ - $\pi$  interaction and electrostatic attraction as well. For pure MnO<sub>2</sub>, significant XRD diffraction peaks were recorded at  $2\theta = 22.3$ ,  $37.2$ , and  $42.7^\circ$ , and could be well-assigned to the (120), (131), and (300) planes of  $\gamma$ -MnO<sub>2</sub> (JCPDS 14-644), respectively. It should be noted that the PANI and PANI-based composites have no characteristic peaks at  $2\theta$  of  $37.2^\circ$  and  $42.7^\circ$  compared with pure MnO<sub>2</sub>. And because MnO<sub>2</sub> is only a minor oxidant, there is no residue in the PANI and PANI based composites.

Figure 4 is an XPS characterization of PANI/GO (all PANI and PANI-based composites were prepared by in situ chemical oxidative polymerization procedures, so it was only proved that no residual MnO<sub>2</sub> in PANI/GO could prove that other materials had no MnO<sub>2</sub> residue.). In the survey spectrum, peaks of O 1s, N 1s, and C 1s are clearly visible at 530.9, 398.0, and 284.7 eV, respectively. However, the Mn 2p 3/2 peak at 642.1 eV and the Mn 2p 1/2 peak at 653.7 eV are absent, which is in good agreement with our assumption that MnO<sub>2</sub> should not be present in the electrode material.

The morphology of GO, GO-NaBH<sub>4</sub>, PANI/GO, and PANI/GO-NaBH<sub>4</sub> was analyzed by field emission scanning electron microscopy (FE-SEM). Figure 5a is a scanning

**Fig. 4** XPS spectrum of PANI/GO sample



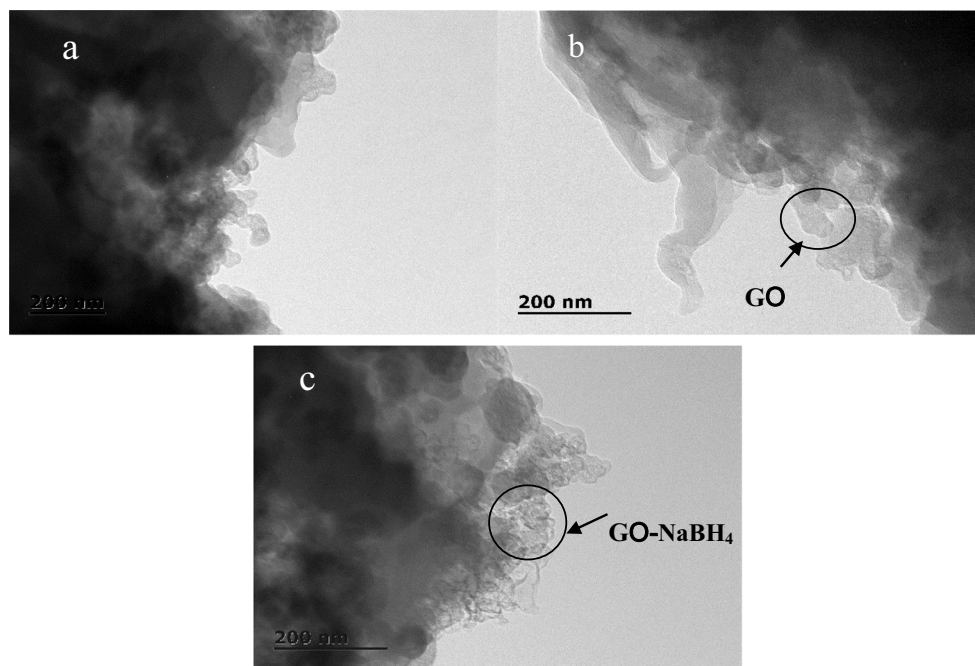


**Fig. 5** Scanning electron micrograph of field emission of PANI and PANI/graphene composites. **a** GO. **b** GO-NaBH<sub>4</sub>. **c** PANI. **d** and **e** PANI/GO. **f** PANI/GO-NaBH<sub>4</sub>

electron micrograph of graphene oxide, and Fig. 5b is a graph of graphene oxide with a low degree of oxidation after being reduced by NaBH<sub>4</sub>. It can be seen from the picture that the graphene synthesized by the modified Hummers method is a half transparent pleated structure, a microcrystalline structure which is corrugated and stacked on each other, and has a large specific surface area; Fig. 5c is a FE-SEM image of PANI, which exhibits irregular granules. We can see that the agglomeration of PANI is more serious because of the growth of PANI after nucleation during chemical oxidation, and the way of growth is to wrap a layer in a layer, which leads to

poor dispersion; Fig. 5d and e show the morphology of PANI after incorporation of 2% of GO. The part showing obvious fold structure is graphene; graphene is used as support material, and aniline is in graphene. The surface is polymerized to form PANI, which is caused by the  $\pi$ - $\pi$  interaction between PANI and GO. Simply speaking, PANI is polymerized by using graphene oxide as a template. Figure 5e shows that the size of the material becomes smaller, and the particles are more distinct, which means that the addition of GO can provide more multiple polymerization sites for aniline, and GO caused PANI to change from large particles to small particles

**Fig. 6** TEM image of PANI and PANI/graphene composites. **a** PANI. **b** PANI/GO **c** PANI/GO-NaBH<sub>4</sub>



and reduced agglomeration. Figure 5f is a scanning electron micrograph of PANI/GO-NaBH<sub>4</sub>. Similar to PANI/GO, GO-NaBH<sub>4</sub> provides more polymerization active sites for the synthesis of PANI, which weakens the agglomeration of PANI and further makes the transfer process of ions smoother.

Figure 6a is a TEM image of PANI; we can clearly see that PANI nanoparticles are clustered together; Fig. 6b is a PANI/GO transmission electron micrograph, which is oxidized due to less doping of GO; most of the graphene has been covered by PANI, and only a small part is exposed, showing a thin wrinkle structure; PANI and GO are combined by  $\pi$ - $\pi$  interaction; Fig. 6c is a transmission electron microscopy image of PANI/GO-NaBH<sub>4</sub>, which is almost the same as the morphology of PANI/GO. The PANI at the edge is thinner and

translucent. The internal PANI is thicker, and the surface of graphite is covered by PANI.

### Electrochemical properties

The alternating current (AC) impedance spectra of conductive polymers were used to study film conductivity, structure, and charge transport in the polymer film interface. The electrochemical impedance spectrum has a frequency range of  $10^{-2}$  to  $10^5$  Hz and a sinusoidal voltage AC amplitude of 5 mV. Figure 7 shows a comparison of Nyquist plots of PANI, PANI/GO, and PANI/GO-NaBH<sub>4</sub>. It can be seen that the addition of graphene greatly reduces the resistance of the battery. At lower frequencies, the Nyquist plot of composites is more vertical than PANI. At higher frequencies, the composite electrode exhibits a relatively small radius.

In order to better analyze the changes of the resistance of each part, the Nyquist diagram is fitted by ZSim Demo software. The equivalent circuit is shown in Fig. 8, where  $R_s$  represents the solution resistance,  $R_{CT}$  is the charge transfer resistance, and  $C$  is electric double layer capacitance, and the fitting results are shown in Table 1. As can be seen from Table 1, the difference in solution resistance of the battery is not large, which is related to the conductivity of the

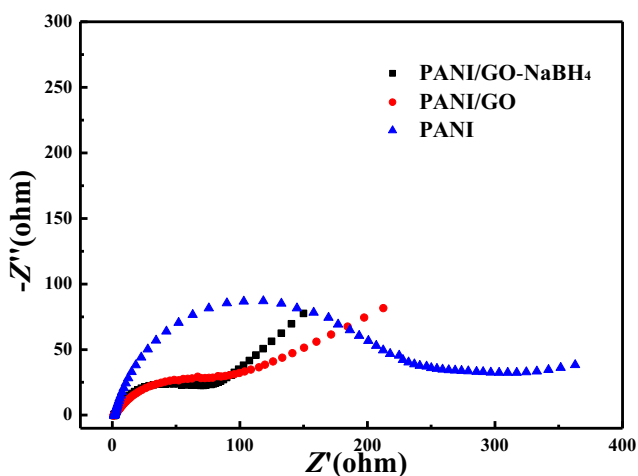


**Fig. 7** EIS spectrum of PANI and PANI/graphene composites (PANI, PANI/GO, and PANI/GO-NaBH<sub>4</sub>)

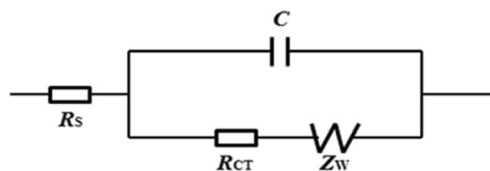


**Fig. 8** Equivalent circuit diagram of Zn/PANI rechargeable battery

**Table 1** Nyquist plot fitting results of Zn/PANI rechargeable battery

Sample	$R_s$ (ohm)	$C$ (F)	$N$ ( $0 < n < 1$ )	$R_{CT}$ (ohm)	$W$
PANI	7.665	$1.62 \times 10^{-3}$	0.8505	226.8	0.0826
PANI/GO	6.222	$3.0 \times 10^{-5}$	0.6863	120.2	0.03692
PANI/GO-NaBH <sub>4</sub>	4.835	$2.07 \times 10^{-5}$	0.6234	105.4	0.02436

electrolyte, but the charge transfer resistance  $R_{CT}$  is significantly reduced. The charge transfer resistance of PANI is 226.8  $\Omega$ , and the charge transfer resistance of PANI/GO and PANI/GO-NaBH<sub>4</sub> is 120.2  $\Omega$  and 105.4  $\Omega$ , respectively, which fully demonstrates that the electrochemical activity of the PANI/graphene composite is higher. Since PANI does not have sufficient polymerization sites during the polymerization process, it will proliferate continuously on the formed PANI core and polymerize in the form of layered coating, which leads to agglomeration phenomenon, which is not conducive to the sufficient material and electrolyte. Doped with graphene oxide, PANI and graphene are combined by  $\pi$ - $\pi$  interaction, so that aniline is polymerized with graphene as a template, and this 3D hybrid nanostructure provides greater porous structure and electrical conductivity.

The electrochemical activity and cycle performance of PANI and PANI/graphene composites were further tested by cyclic voltammetry. PANI and its composites were working electrodes. Zinc was used as the counter electrode. The potential window was 0.3 V~1.7 V (Vs Zn/Zn<sup>2+</sup>) with a scan speed of 0.5 mV/s.

As shown in Fig. 9, the cyclic voltammetry curve of PANI shows obvious oxidation peaks (corresponding to the permeation of perchlorate ions) and reduction peaks (corresponding to the permeation of perchlorate ions at 1.3 V and 0.8 V, respectively [33]), indicating that the material has good redox

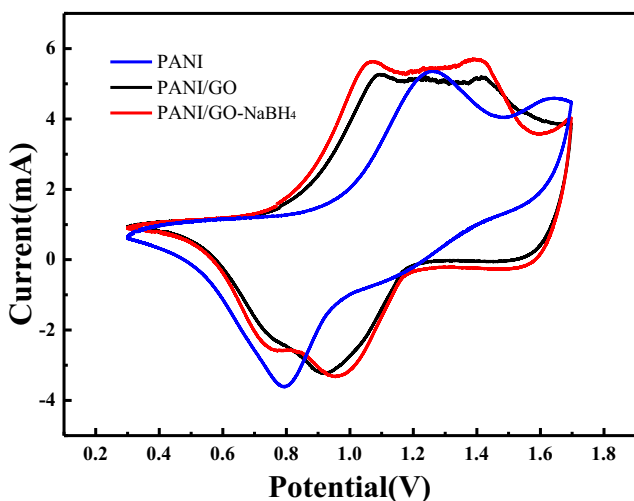


**Fig. 9** CV curve of PANI and PANI/graphene composites (PANI, PANI/GO, and PANI/GO-NaBH<sub>4</sub>)

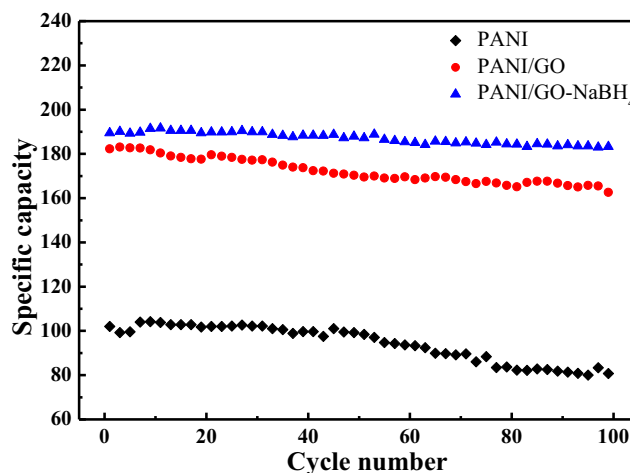


**Fig. 10** Relationship between specific capacity and cycle number of PANI and PANI/graphene composites (PANI, PANI/GO, and PANI/GO-NaBH<sub>4</sub>)

properties. After being compounded with graphene, the current density and curve area of the composite are much larger than that of PANI at the same sweep speed. The oxidation potential is between 1.1 V and 1.4 V, and the reduction potential is between 0.7 V and 1.0 V. The peak shape can be clearly seen as a partial overlap of the two pairs of oxidation peak reduction peaks, which indicates that the perchlorate ion insertion and removal on the positive and negative electrodes are carried out in two steps, which are PANI and graphene play a synergistic result. Graphene provides more active sites for PANI polymerization. The specific surface area of the electrode material is increased to facilitate contact with the electrolyte. The layered and short fiber-like structure shortens the diffusion distance of ions in the electrolyte.

The cycle performance of PANI and PANI/graphene composites was investigated by a 0.2 C constant current charge and discharge cycle 100 times. Figure 10 shows the specific capacity-cycle number curves of PANI, PANI/GO, and PANI/GO-NaBH<sub>4</sub>. It can be seen that the discharge capacity of PANI/GO and PANI/GO-NaBH<sub>4</sub> is greatly improved compared with PANI.

PANI is used as the positive electrode of the battery, and the max discharge specific capacity reaches 100 mAh/g. After 100 cycles, the capacity remains at 80.4%. After a small amount of GO was added, the highest discharge capacity reached 183 mAh/g; after 100 cycles, the capacity was attenuated to 163.62 mAh/g, and the capacity retention rate was 89.4%. After the low oxidation degree of GO reduced by NaBH<sub>4</sub>, the highest discharge specific capacity reached 192 mAh/g, and the specific discharge capacity of the 100th charge and discharge cycle was 182.5 mAh/g; the capacity retention rate was 95.05%. During the synthesis process, PANI particles are aggregated into large clusters, resulting in lower specific surface area and low conductivity. Graphene materials have excellent electron conductivity, large specific

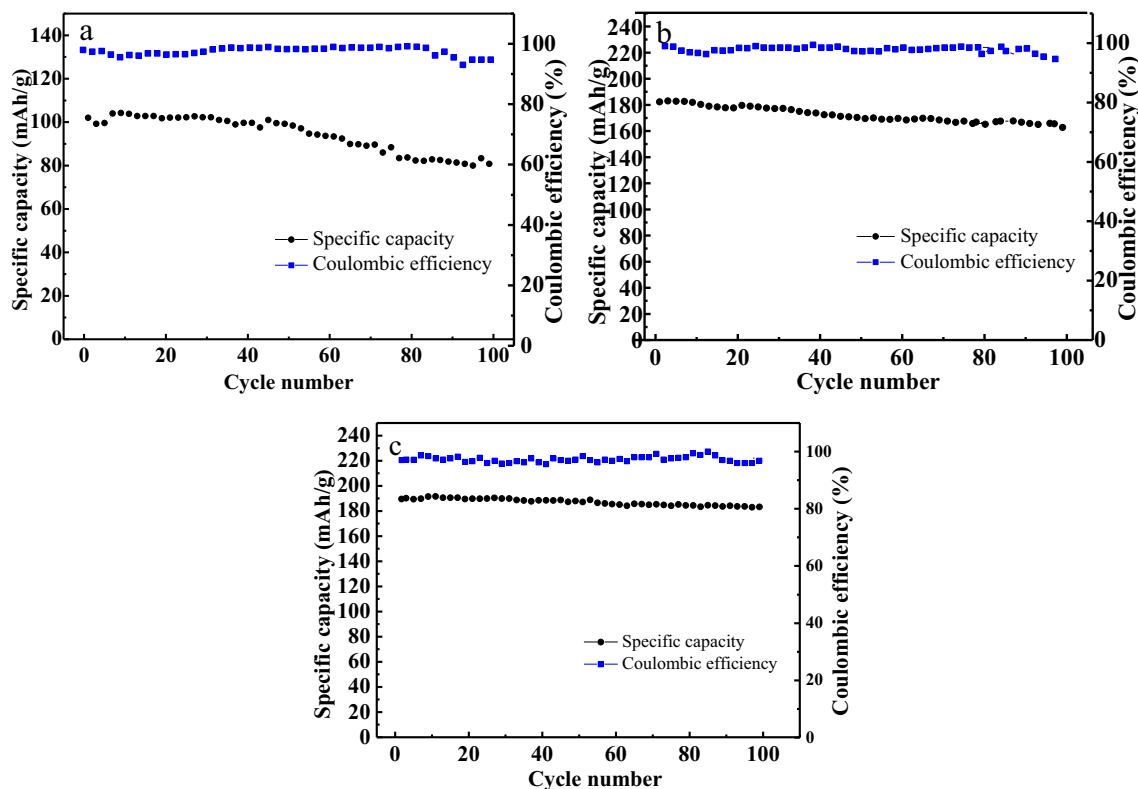


**Fig. 11** Relationship between specific capacity, coulombic efficiency, and cycle number of PANI and PANI/graphene composites. **a** PANI. **b** PANI/GO. **c** PANI/GO-NaBH<sub>4</sub>

surface area, and good mechanical properties. Two percent graphene oxide is added before oxidative polymerization, and aniline polymerizes with graphene as a template, which reduces the agglomeration of PANI and improves the conductivity of the PANI material. In addition, this unique package structure provides more active sites for electrochemical reactions and the  $\pi$ - $\pi$  interaction between graphene and PANI is more favorable for ion dedoping. At the same time, the presence of GO and GO-NaBH<sub>4</sub> prevents the expansion and

contraction of PANI during repeated charge and discharge cycles, resulting in damage to the mechanical structure, thereby improving the cycle performance of PANI/GO, and PANI/GO-NaBH<sub>4</sub>.

Figure 11 a, b, and c are PANI, PANI/GO, and PANI/GO-NaBH<sub>4</sub> as the positive electrode material of zinc rechargeable battery, the specific capacity and coulombic efficiency with the number of cycles. The coulombic efficiency of PANI battery is more than 90% after a period of cycle, but the coulomb efficiency drops rapidly after 80 cycles; after the addition of GO, the coulomb efficiency is mostly above 95%, indicating that the reversibility of the material has significant improvement. The coulombic efficiency of PANI/GO-NaBH<sub>4</sub> is basically above 95% after reaching stability.

In order to test the rate performance of PANI-based composites, the batteries were charged and discharged at 0.1 C, 0.2 C, 0.5 C, 1 C, and 0.1 C using a LAND electric charge and discharge test system. Figure 12 shows the rate charge and discharge test chart of PANI, PANI/GO, and PANI/GO-NaBH<sub>4</sub>; PANI is difficult to achieve normal charge and discharge at 0.5 C and 1 C; the battery capacity is particularly low, which is difficult to meet the requirements of ion dedoping. After doping with GO and GO-NaBH<sub>4</sub>, the specific discharge capacity at 0.5 C is 166.1 mAh/g and 179.2 mAh/g, respectively; the specific current charge and discharge capacity at 1 C is 147.8 mAh/g and 157.75 mAh/g, respectively.

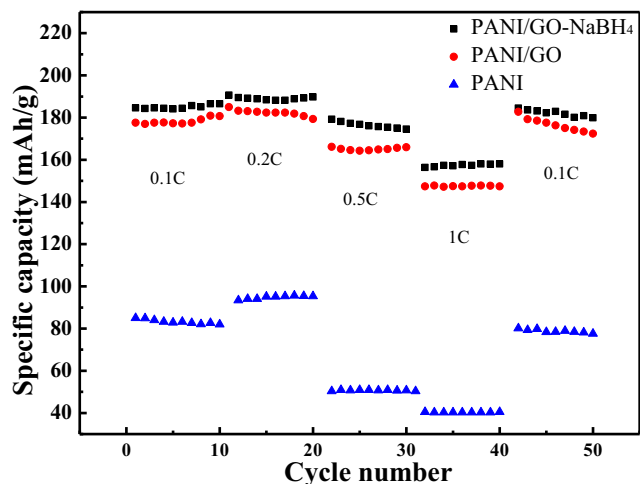


**Fig. 12** Rate performance test of PANI and PANI/graphene composites (PANI, PANI/GO, and PANI/GO-NaBH<sub>4</sub>)



The rate of discharge of graphene oxide with a low degree of oxidation is slightly higher than that of GO. This is because the conductivity and specific surface area of graphene are improved to some extent after the reduction of graphene oxide by  $\text{NaBH}_4$ .

## Conclusion

PANI/graphene composites were synthesized by a new in situ chemical oxidative polymerization method. The physical properties and chemical characterization prove that the synthesis of the composite material optimizes the performance of the battery.

After the incorporation of graphene, the charge transfer resistance is significantly reduced; the area of the cyclic voltammetry curve and the current density are significantly increased. Electrochemical characterization tests show that the electrochemical properties of the composite material are significantly improved. We synthesized three composites of PANI, PANI/GO, and PANI/GO- $\text{NaBH}_4$ , and the specific discharge capacity increased from 100 to 183 mAh/g and 192 mAh/g, respectively. These results illustrate that this kind of composite will have broad prospects as a cathode material for zinc/PANI cells in the future.

## References

- Ciric-Marjanovic G (2013) Recent advances in polyaniline composites with metals, metalloids and nonmetals. *Synth Met* 170: 31–56
- Xia C, Guo J, Lei Y, Liang H, Zhao C, Alshareef (2017) Rechargeable aqueous zinc-ion battery based on porous framework zinc pyrovanadate intercalation cathode. *Adv Mater* 30: 1705580
- Nuramdhani I, Gokceoren AT, Odhiambo SA, De MG, Hertleer C, Van LL (2018) Electrochemical impedance analysis of a pedot: pss-based textile energy storage device. *Materials* 11:48
- Cheng C, Rui X, Shen W (2018) A lithium-ion battery-in-the-loop approach to test and validate multi-scale dual H infinity filters for state of charge and capacity estimation. *IEEE Trans Power Electron* PP:1–1
- Wang H, Tao Z, Fu Y, Xiao H, Bai H (2019) Research on influencing factors for consistency performance of lithium ion batteries. *IOP Conf Ser Earth Environ Sci* 223:012–036
- Nordrum A (2019) A safer way for batteries to fail: putting a gap in the right place can stop lithium-ion batteries from exploding. *IEEE Spectr* 56:12–13
- Liu G, Yu Y, Jing H, Wei X, Liu X, Liu Y (2014) An ecological risk assessment of heavy metal pollution of the agricultural ecosystem near a lead-acid battery factory. *Ecol Indic* 47:210–218
- Liu X, Cai JC, Shu YH (2014) The elimination of pollution of toxic cadmium and arsenic in lead-based alloys of lead-acid batteries in China. *Adv Mater Res* 983:319–323
- Xu C, Li B, Du H, Kang F (2012) Energetic zinc ion chemistry: the rechargeable zinc ion battery. *Angew Chem* 51(4):933–935
- Kundu D, Adams BD, Duffort V, Vajargah SH, Nazar LF (2016) A high-capacity and long-life aqueous rechargeable zinc battery using a metal oxide intercalation cathode. *Nat Energy* 1:16119
- Zhang L (2017)  $\text{Mn}_3\text{O}_4$ /carbon nanotube nanocomposites recycled from waste alkaline Zn– $\text{MnO}_2$  batteries as high-performance energy materials. *Rare Metals* 36:442–448
- Sun W (2017) Zn/ $\text{MnO}_2$  battery chemistry with  $\text{H}^+$  and  $\text{Zn}^{2+}$  coinserion. *J Am Chem Soc* 139(29):9775–9778
- Mones ES, Gillado AV, Herrera MU (2016) Photoresponse of zinc oxide-polyaniline junction at different light intensities. *Key Eng Mater* 705:4
- Rafiqi FA, Majid K (2016) Synthesis, characterization, photophysical, thermal and electrical properties of composite of polyaniline with zinc bis (8-hydroxyquinolate): a potent composite for electronic and optoelectronic use. *RSC Adv* 6:22016–22025
- Kan J, Xue H, Mu S (1998) Effect of inhibitors on Zn-dendrite formation for zinc-polyaniline secondary battery. *J Power Sources* 74:113–116
- Huang J, Zhuo W, Hou M (2018) Polyaniline-intercalated manganese dioxide nanolayers as a high-performance cathode material for an aqueous zinc-ion battery. *Nat Commun* 9:2906
- Wang X, Xin J, Dawei GU, Shen L (2006) A novel Zn-PANI dry rechargeable battery. *Rare Metals* 25:67–70
- Mohsen RM, Morsi SMM, Selim MM, Ghoneim AM, El-Sherif HM (2018) Electrical, thermal, morphological, and antibacterial studies of synthesized polyaniline/zinc oxide nanocomposites. *Polym Bull* 76:1–21
- Ghanbari K (2007) Synthesis of polyaniline/graphite composite as a cathode of Zn-polyaniline rechargeable battery. *J Power Sources* 170:513–519
- Dizon JCM, Tapia AKG, Razado-Colambo I, Herrera MU (2018) Fabrication of polyaniline on silane-functionalized zinc oxide. *Key Eng Mater* 775:94–98
- Liu P (2017) Polyaniline/multi-walled carbon nanotubes composite with core-shell structures as a cathode material for rechargeable lithium-polymer cells. *Appl Surf Sci* 400:446–452
- Fonseca BL, Fonseca MA, Oliveira MSA (2018) Thermo-mechanical characterization of shape-memory polyurethane nanocomposites filled with carbon nanotubes and graphene nanosheets. *Polym Compos* 39:1216–1223
- Chen C, Xi J, Zhou E, Li P, Chen Z, Chao G (2018) Porous graphene microflowers for high-performance microwave absorption. *Nano-Micro Letters* 10:26
- Moreno C, Vilas-Varela M, Kretz B, Garcia-Lekue A, Costache MV, Paradinas M (2018) Bottom-up synthesis of multifunctional nanoporous graphene. *Science* 360:199–203
- Gupta RK, Alahmed ZA, Yakuphanoglu F (2013) Graphene oxide based low cost battery. *Mater Lett* 112:75–77
- Farooqui UR, Ahmad AL, Hamid NA (2018) Graphene oxide: a promising membrane material for fuel cells. *Renew Sust Energ Rev* 82:714–733
- Dreyer DR, Park S, Bielawski CW (2010) The chemistry of graphene oxide. *Chem Soc Rev* 39(1):228–240
- Weijie W, Jian Y, Jiaqin L, Dawei O, Qingqing Q, Binbin L (2018) Self-healing polyaniline-graphene oxides based electrodes with enhanced cycling stability. *Electrochimica* 282:835–844
- Harfouche N, Gospodinova N, Nessark B, Perrin FX (2017) Electrodeposition of composite films of reduced graphene oxide/polyaniline in neutral aqueous solution on inert and oxidizable metal. *J Electroanal Chem* 786:135–144
- Almeida DAL, Couto AB, Ferreira NG (2019) Flexible polyaniline/reduced graphene oxide/carbon fiber composites applied as electrodes for supercapacitors. *J Alloys Compd* 788:453–460
- Saha S, Mitra M, Sarkar A, Banerjee D, Ganguly S, Kargupta K (2018) Lithium assisted enhanced hydrogenation of reduced

- graphene oxide-PANI nanocomposite at room temperature. *Diam Relat Mater* 84:103–111
32. Shi HY, Ye YJ, Liu K, Song Y, Sun X (2018) A long cycle-life self-doped polyaniline cathode for rechargeable aqueous zinc batteries. *Angew Chem Int Ed* 57(50):16359–16363
  33. Ji C, Yao B, Li C, Shi G (2013) An improved Hummers method for eco-friendly synthesis of graphene oxide. *Carbon* 64:225–229
  34. Guerrero-Contreras J, Caballero-Briones F (2015) Graphene oxide powders with different oxidation degree, prepared by synthesis variations of the Hummers method. *Mater Chem Phys* 153:209–220
  35. Zhang P, Han X, Kang L, Qiang R, Liu W, Du Y (2013) Synthesis and characterization of polyaniline nanoparticles with enhanced microwave absorption. *RSC Adv* 3:12694
  36. Remyamol T, John H, Gopinath P (2013) Synthesis and nonlinear optical properties of reduced graphene oxide covalently functionalized with polyaniline. *Carbon* 59:308–314

**Publisher's note** Springer Nature remains neutral with regard to jurisdictional claims in published maps and institutional affiliations.